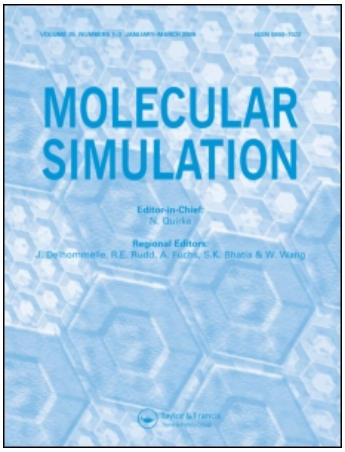

Molecular Simulation
Publication details, including instructions for authors and subscription information:
http://www.informaworld.com/smpp/title~content=t713644482

Metal nanocrystal-seeded synthesis of carbon nanotubes and nanofibers in a supercritical fluid

Doh C. Lee[a]; Brian A. Korgel[a]
[a] Department of Chemical Engineering, Texas Materials Institute and Center for Nano- and Molecular Science and Technology, The University of Texas, Austin, TX, USA

To cite this Article Lee, Doh C. and Korgel, Brian A.(2005) 'Metal nanocrystal-seeded synthesis of carbon nanotubes and nanofibers in a supercritical fluid', Molecular Simulation, 31: 9, 637 — 642
To link to this Article: DOI: 10.1080/08927020500108023
URL: http://dx.doi.org/10.1080/08927020500108023

Molecular Simulation, Vol. 31, No. 9, August 2005, 637–642

Taylor & Francis
Taylor & Francis Group

Metal nanocrystal-seeded synthesis of carbon nanotubes and nanofibers in a supercritical fluid

DOH C. LEE and BRIAN A. KORGEL*

Department of Chemical Engineering, Texas Materials Institute and Center for Nano- and Molecular Science and Technology, The University of Texas, Austin, TX, 78712-1062, USA

(Received November 2004; in final form December 2004)

Multiwall carbon nanotubes (MWNTs) were formed in supercritical toluene using ferrocene to promote their growth. The crude reaction product is comprised of a mixture of MWNTs and carbon nanofilaments. The morphological difference in the products, i.e. MWNTs versus carbon nanofilaments, appears to originate from the dependence of the growth mechanism on the particle size, with seed particles larger than ~30 nm in diameter producing filaments and smaller particles producing MWNTs.

Keywords: Carbon nanotubes; Supercritical fluid; Electron energy-loss spectroscopy; Growth mechanism

1. Introduction

It has been known since at least 1955 [1] that certain metals, such as iron, cobalt and nickel, catalyze the formation of carbon nanofibers and possibly nanotubes, and the intentional synthesis of carbon nanofibers and nanotubes has been studied and developed for more than a decade [2]. However, it is only during the last several years that metal seed particles have been used to catalyze the growth of high quality single-wall and multiwall carbon nanotubes (SWNTs and MWNTs) at relatively low temperature (500–800°C) by chemical vapor deposition (CVD) [3,4]. Although CVD growth can be quite effective, nanotube formation occurs on a substrate surface in a batch synthetic processes, which limits the product yield and throughput. For microelectronics applications, and other high value-added applications, such as high-resolution displays, this may not be an issue. However, for other applications such as fabrics and structural composites that require large amounts of nanotubes at low cost, an alternative high throughput synthetic process is needed.

During recent years, we have pioneered the supercritical fluid–liquid–solid (SFLS) synthesis of semiconductor nanowires [5–9]. The process utilizes sterically-stabilized metal nanocrystals as seeds to crystallize semiconductor nanowires in a solvent heated and pressurized above its critical point. A solution of molecular precursor fed with the metal nanocrystals into a pressurized reactor at a temperature exceeding the metal: semiconductor eutectic temperature decomposes and dissolves in the seed particle to ultimately form nanowires [10]. Unlike in the CVD process, nanowires are produced homogeneously in the solvent and a continuous high throughput of nanowires is possible. Recently, we extended the SFLS approach to the synthesis of carbon nanotubes using toluene as a carbon nanotube precursor and ferrocene as a molecular precursor that forms iron nanocrystals in the reactor to seed nanotube growth [11]. Here, we discuss in detail the carbon nanotube growth mechanism in this process and the relationship between the product morphology and the size of the seed particle. In contrast to SFLS growth, the nanotubes and fibers are produced from a solid Fe or Fe_3C seed, and therefore we call this process supercritical fluid–solid–solid (SFSS) growth.

2. Experimental

A 10 mL stainless-steel high-pressure cell is loaded in a nitrogen-filled glove box with a 2.5 ml solution of ferrocene in toluene. The sealed reactor is removed from the glovebox

*Corresponding author. Email: korgel@mail.che.utexas.edu

Molecular Simulation
ISSN 0892-7022 print/ISSN 1029-0435 online © 2005 Taylor & Francis Group Ltd
http://www.tandf.co.uk/journals
DOI: 10.1080/08927020500108023

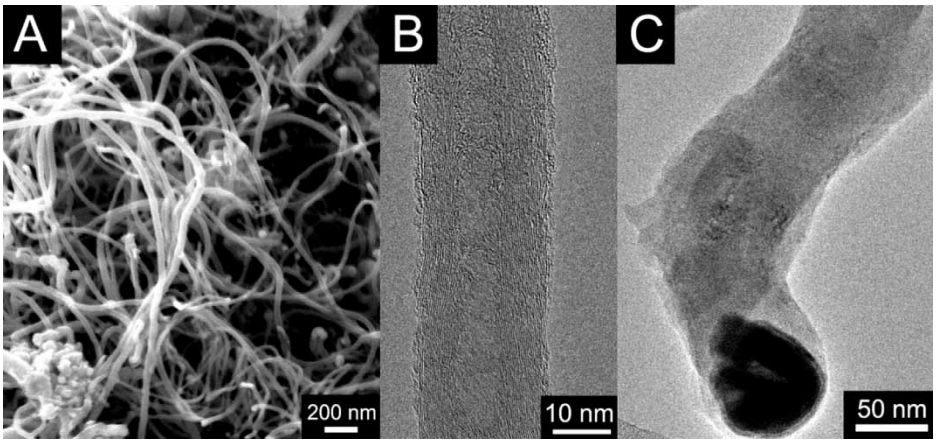

Figure 1. (A) High-resolution scanning electron microscopy (HRSEM) image of the crude reaction product comprised of MWNTs and carbon nanofilaments. The batch reaction was performed with 2.5 mM ferrocene in toluene solution for 15 min at 600°C and ~12.4 MPa. HRTEM image of (B) a multiwall carbon nanotube (MWNT) and (C) a carbon nanofilament show that MWNTs have coaxial stacking of graphene layers along the length of growth axis, and carbon nanofilaments exhibit disordered stacking of graphitic sheets.

and placed into a heating block that has been preheated to a temperature approximately 60°C higher than the reaction temperature. The volume of solution initially loaded in the reactor determines the pressure, which can be deduced from the phase diagram for toluene [12]. Note that caution should be taken to avoid exceeding the pressure rating on the reactor. A reaction carried out at 600°C and ~12.4 MPa for 15 min with 2.5 mM solution of ferrocene in toluene provided the carbon nanotubes. The reactor is removed from the heating block after 15 min and then cooled rapidly in an ice water bath. After reaching room temperature, the reactor seal is carefully broken and the product extracted in hexane with mild ultrasonic agitation.

High-resolution scanning electron microscopy (HRSEM) was used to obtain an initial assessment of the raw product morphology. The crude materials collected in hexane were drop-cast on a $2 \times 2\,cm^2$ silicon wafer HRSEM images were obtained on a field emission LEO 1530 SEM operated at the accelerating voltage of 4 kV. High-resolution transmission electron microscopy (HRTEM) on the reaction product was performed using a JEOL 2010F operating at 200 kV accelerating voltage. For imaging, the nanotubes were drop cast from hexane onto lacey carbon-coated TEM grids (Electron Microscopy Sciences). Electron energy loss spectroscopy (EELS) was performed on the JEOL 2010F TEM equipped with a Gatan parallel-EELS spectrometer. Electron energy loss spectra were acquired in STEM mode with the field emission gun operating at 200 keV, the EELS aperture size set at 2 nm, and a camera length of 10 cm, which translates into 5 mrad of collection semi-angle. The use of lacey carbon grids as substrates enables nanotubes to be

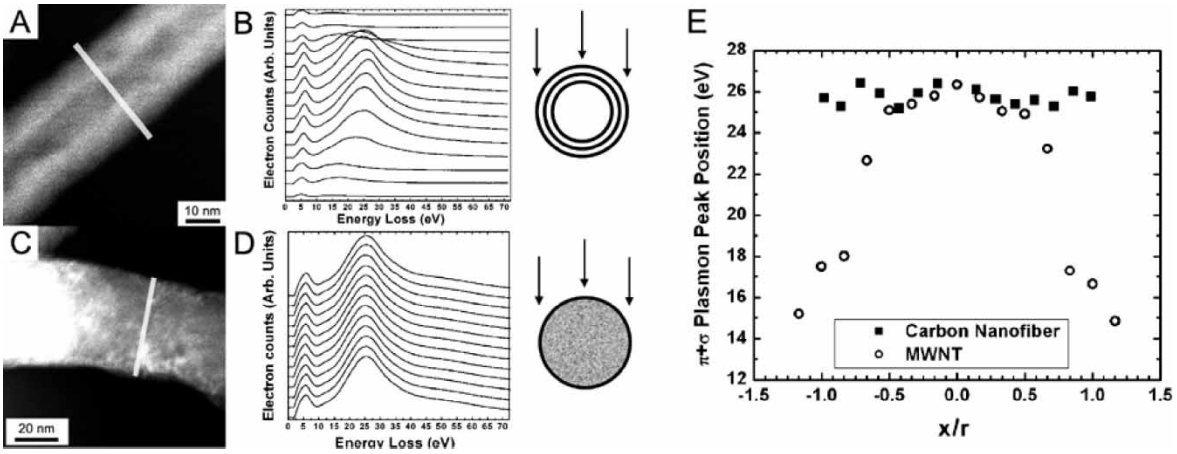

Figure 2. Scanning transmission electron microscopy (STEM) mode images of (A) a MWNT and (C) a carbon nanofilament, taken using dark-field detector. EELS line scans across the individual nanostructures are shown in (B) and (D), respectively. The angular dependence is depicted in corresponding schematics, and the $\pi + \sigma$ plasmon peak positions as a function of probe position are plotted in (E). The peak position depends upon the way of graphene layer stacking.

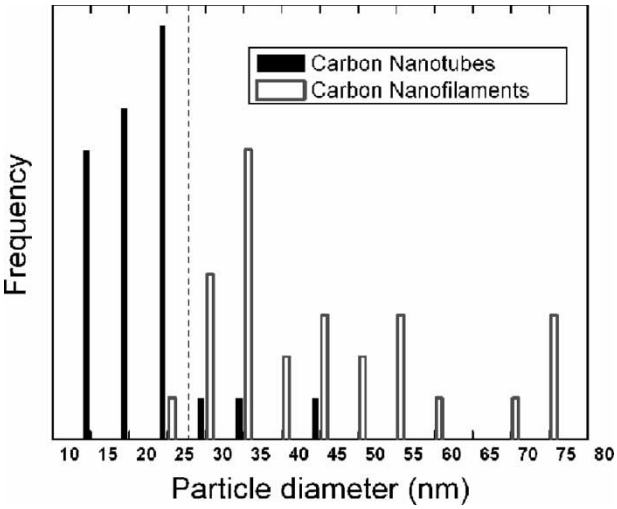

Figure 3. Size distribution of the particle size at the tip of carbon nanotubes (filled) and carbon nanofilaments (hollow). Very few MWNTs are observed with metal particles at their tips with diameters larger than 25 nm (dashed line), and no fibers were observed with metal particles at their tips smaller than 23 nm. Data was sampled from images of 60 nanotubes and nanofibers.

suspended over a vacuum background, which ensures the absence of a background carbon signal that would obscure the spectroscopic data.

3. Results and discussion

3.1. Ferrocene-catalyzed growth of MWNTs and nanofilaments

Figure 1A shows an SEM image of the carbonaceous product obtained by reacting 2.5 mM ferrocene in toluene at 600°C and ~12.4 MPa. The SEM shows the mesh of wiry product that forms in the reaction. TEM imaging reveals that two morphologies are produced in the reaction: MWNTs (figure 1B) and nanoscale carbon filaments (figure 1C). Both MWNTs and the solid filaments are composed of layered graphene sheets. However, the MWNTs exhibit graphene sheets wrapped concentrically around the hollow interior of the tube, while filaments are comprised of a solid core of randomly stacked graphene sheets. In the filaments, the graphene layers are barely distinguishable from an amorphous structure, yet the random stacking structure is characteristic of filaments grown using catalytic seed particles. In the MWNTs, the spacing (~0.344 nm) measured by TEM between neighboring graphene tubules matches well the expected interlayer separation (~0.341 nm) in MWNTs determined by neutron diffraction [13].

EELS is a powerful method for distinguishing between carbon nanotubes and filaments. It is one technique that enables microscopic structural details of an individual nanostructure to be correlated with its electronic properties. Even more interestingly, the electronic properties can be *mapped* spatially in a single nanostructure because the electron probe can be reduced to a diameter of 0.5 nm and scanned across the nanostructure. Figure 2 shows EELS line scans on a MWNT (figure 2A) and a filament (figure 2C). In the low loss region of the spectra shown, two peaks appear that correspond to inelastic scattering from π (~6 eV) and $\pi + \sigma$ (~26 eV) valence electrons [14]. In the MWNT, the increasing curvature of the ordered graphene layers at the outside of the nanotube increases the incident angle of the electron beam and the graphene sheet as the probe is moved from the center of the nanotube to the radial edge. The change in incident angle results in a shift of the $\pi + \sigma$ peak to lower energy from ~27 to ~15 eV, which is very close to the values of ~27 to ~19 eV measured by Zeppenfeld for a change from perpendicular to parallel incident angle with respect to a graphite sheet [15]. Since the graphene layers are disordered in the filament, the angle of incidence between the graphene sheet orientation and the electron beam does not depend on the radial position in the filament and therefore the $\pi + \sigma$ peak does not change with position [15]. The $\pi + \sigma$ peak shift in the EELS data provides a clear indication that MWNTs are formed in the synthesis.

3.2. MWNT and filament growth mechanism

Both MWNTs and carbon nanofilaments are produced in toluene at 600°C in the presence of ferrocene. Without the addition of ferrocene, toluene is chemically stable under these conditions and does not decompose. Therefore, ferrocene plays a catalytic role in aiding toluene decomposition to carbon; however, ferrocene decomposes rapidly at 600°C to form Fe nanocrystals, and these nanocrystals are most likely the catalytically active species, as it is well known that Fe metal particles are effective catalysts for decomposing hydrocarbons to graphite [16–19]. As toluene decomposes on the Fe nanocrystal surface, either MWNTs or filaments form. The morphology of the carbonaceous product appears to depend on the Fe seed particle size, with seed particles larger than ~25 nm producing filaments and smaller particles leading to MWNTs. High-magnification TEM images of the metal seed particles remaining at the ends of MWNTs and filaments reveal significant differences in crystallographic structure and composition that depends on the carbon morphology. The seed particles at the MWNT tips exhibit crystallinity characteristic of bcc Fe metal; whereas, the seed particles imaged at the filament tips have a core-shell structure that appears to be associated with Fe–C alloys of two different compositions or crystal structures, with the core alloy closest to Fe_3C (cementite) [11].

During the synthesis of both MWNTs and filaments, toluene decomposes on the Fe particle surface to provide a continuous supply of carbon to the seed. Metal surface-induced carbidization and graphitization are well-established processes in nanotube or nanofilament growth from various metals, including Fe [19], Co [20], Ni [21], or bimetallic alloys, such as Fe/Ru [22]. Yet, the precise

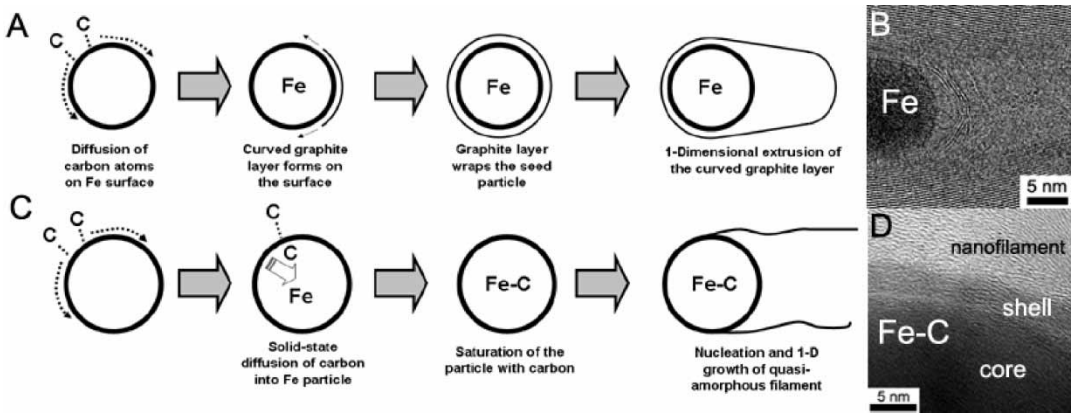

Figure 4. Schematic growth mechanisms for (A) carbon nanotubes and (C) carbon nanofilaments are exhibited. MWNTs observed in this study typically exhibit structures characteristic of the "folded growth mechanism", although few examples of nanotubes that appear to have grown via the "root growth mechanism" have been found (See figure 4C). The root growth mode places a higher surface energy requirement on the nanotube/metal interface, which is not accommodated at the reaction temperature of 600°C. Close-up HRTEM images of seed particles embedded at the tip of a MWNT and a filament, revealing different crystallinities. The seed particle that initiates nanotube growth has the crystalline structure of Fe, whereas the particle that directs nanofilament growth has structure of Fe–C alloy.

growth mechanisms of SWNTs, MWNTs and filaments, and the factors that determine the product morphology are not well established.

Both carbon morphologies, the MWNTs and filaments, appear to grow from *solid* metal seeds, as opposed to liquid Fe–C alloyed droplets, as would be the case in a typical SFLS nanowire synthesis. The reaction temperature of 600°C is far below the Fe–C eutectic temperature (1130°C) [23], making it unlikely that Fe and C would form a liquid alloy during the growth process. However,

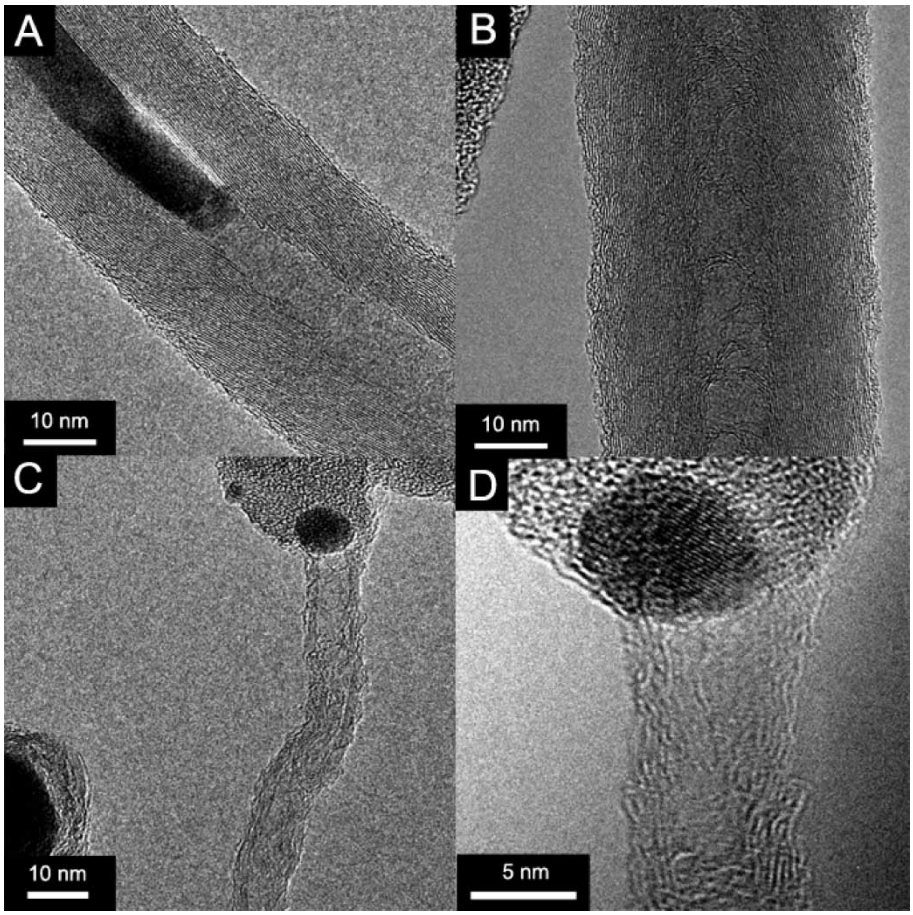

Figure 5. HRTEM images of multiwall carbon nanotubes grown at 600°C and ~12.4 MPa for 15 min with 2.5 mM of ferrocene solution in toluene showing (A) Fe seed particle embedded within the core of nanotube; (B) the bamboo-like structure typical of the MWNTs; and (C, D) the Fe tip at the end of what looks to be a "root-grown" nanotube.

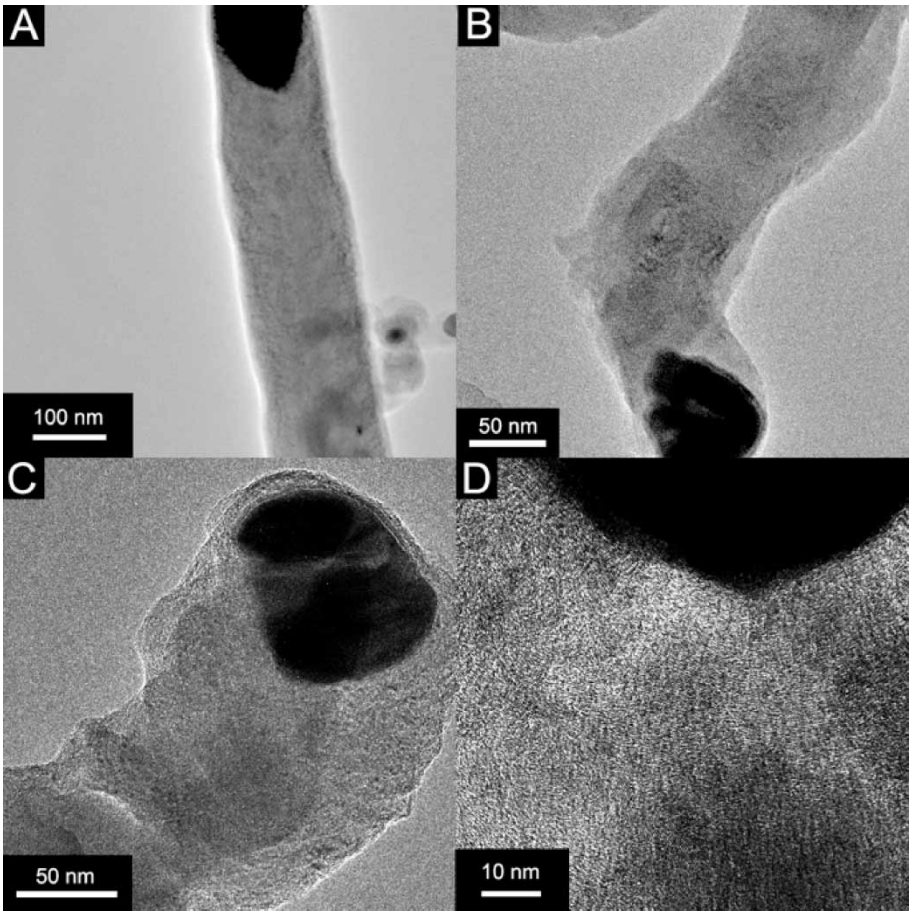

Figure 6. Nanofilaments produced simultaneously with the MWNTs shown in figure 4. TEM images of (A) a carbon filament grown from a ~120 nm size seed particle; (B) a curly filament grown from a ~50 nm particle; and (C) a straight filament grown from a ~50 nm diameter seed particle. (D) Enlarged image in (C) showing the random stacking of graphene layers in the filament.

diffusion and saturation of C into solid Fe is a likely process given that C has a reasonably high solubility in Fe and the diffusive saturation into a sphere 10 nm in diameter occurs in tens of microseconds, and into a 30 nm sphere in milliseconds. An additional driving force for carbon diffusion into the seed particle has been proposed to arise from a temperature gradient from the surface to the particle core created by the exothermic decomposition of hydrocarbon at the particle surface [24,25]. In fact, carbon nanofilaments have been grown on metal nanoparticles at temperatures as low as 525°C, most likely by the VSS mechanism [24]. Carbon diffusion into the solid Fe catalyst particle is one of the key steps to filament growth by SFSS and most likely for MWNT growth as well.

In our study, it appears that the metal seed particle size primarily determines the morphology of the carbon product. From TEM imaging of the metal particles at the ends of 60 filaments and MWNTs, it was found that the metal seed particles were significantly larger for the filaments than the nanotubes. As seen in the histogram of the data in figure 3, very few MWNTs were found associated with particles larger than ~25 nm in diameter; whereas, no filaments were observed with particles at their tips smaller than 23 nm. Two reasons for the morphology dependence on the seed particle size are suggested. First, the Fe seed particle may saturate rapidly with carbon, promoting surface diffusion of decomposing carbon species to the edges of the growing graphene sheets, whereas, the larger particles may promote carbon diffusion into the particle interior, changing the growth mechanism from nanotubes to filaments. Secondly, the nanotubes appear to grow by the "folded-growth" mode, where the graphene sheets wrap around the seed particle, which may be promoted by smaller seed particles (figure 4B). The folded-growth mode is qualitatively different than the "root-growth" mode in which the nanotube ends are actually in contact with the metal surface. Smaller seed particles exhibit a higher surface energy than the larger particles (that give rise to filament growth), which may promote the wrapping of the graphene sheets around it to lower the surface energy. In a few rare cases, for very small nanotubes, metal seed particles appear to have promoted nanotube growth by the root-growth mode, perhaps due to the energetically demanding surface curvature of these very small particles (figure 5C and D). Accordingly, size control

of the metal seed particles in the 10–20 nm diameter size range is a prerequisite for high carbon nanotube selectivity (figure 6).

4. Conclusion

Carbon MWNTs and filaments are produced by Fe nanocrystal-seeded growth in supercritical toluene. This marks a promising first step towards the development of a high throughput solution-phase synthesis of carbon nanotubes. The primary challenge to the process appears to be the stabilization of Fe seed nanocrystals at 600°C in the desired size range to produce MWNTs. Possibly, preformed sterically stabilized nanocrystals could be fed into the reactor as seeds [26] and preliminary research in our laboratory in this direction has shown that MWNTs can be produced but at lower yield, perhaps due to a "blocking effect" of adsorbed hydrocarbon ligands. At any rate, the catalyst particle size appears to determine the morphology of the carbonaceous product and is a critical parameter that must be controlled for success. Another factor that determines the quality of the carbonaceous product—i.e. ratio of MWNTs to filaments, or the production of *single* wall nanotubes—is the reaction temperature. SWNTs were not found in the supercritical toluene synthesis, presumably because the reaction temperature was too low. The problem is that at temperatures much higher than 625°C, toluene homogeneously decomposes very rapidly, competing with heterogeneous nanotube and filament growth to produce large quantities of graphitic byproducts. The byproducts actually appear to poison the metal catalyst particles and prevent nanotube formation under these conditions. Ideally, a supercritical solvent that is thermally stable at higher temperatures, such as CO_2 or water, could provide a promising alternative in which toluene would be fed into the reactor as a reactant with the expectation that it would decompose with a high yield. Our research group has contributed in establishing the chemistry and physics of nanometer-scale materials in supercritical CO_2 and H_2O [10,27], and believe that such a reaction scenario is possible.

Acknowledgements

We thank the National Science Foundation, the Welch Foundation, and the Texas Higher Education Coordinating Board (ATP program) for financial support of this work.

References

[1] L.J. Hofer, E. Sterling, J.T. McCarthy. Structure of the carbon deposited from carbon monoxide on iron, cobalt and nickel. *J. Phys. Chem.*, **59**, 1153 (1955).
[2] J.S. Speck, M. Endo, M.S. Dresselhaus. Structure and intercalation of thin benzene derived carbon fibers. *J. Cryst. Growth*, **94**, 834 (1989).
[3] H. Dai, A.G. Rinzler, P. Nikolaev, A. Thess, D.T. Colbert, R.E. Smalley. Single-wall nanotubes produced by metal-catalyzed disproportionation of carbon monoxide. *Chem. Phys. Lett.*, **260**, 471 (1996).
[4] M.J. Bronikowski, P.A. Willis, D.T. Colbert, K.A. Smith, R.E. Smalley. Gas-phase production of carbon single-walled nanotubes from carbon monoxide via the HiPco process: A parametric study. *J. Vac. Sci. Technol. A*, **19**, 1800 (2001).
[5] J.D. Holmes, K.P. Johnston, R.C. Doty, B.A. Korgel. Control of thickness and orientation of solution-grown silicon nanowires. *Science*, **287**, 1471 (2000).
[6] T. Hanrath, B.A. Korgel. Nucleation and growth of germanium nanowires seeded by organic monolayer-coated gold nanocrystals. *J. Am. Chem. Soc.*, **124**, 1424 (2002).
[7] T. Hanrath, B.A. Korgel. Supercritical fluid–liquid–solid (SFLS) synthesis of Si and Ge nanowires seeded by colloidal metal nanocrystals. *Adv. Mater.*, **15**, 437 (2003).
[8] X. Lu, T. Hanrath, K.P. Johnston, B.A. Korgel. Growth of single crystal silicon nanowires in supercritical solution from tethered gold particles on a silicon substrate. *Nano Lett.*, **3**, 93 (2003).
[9] F.M. Davidson, A.D. Schricker, R. Wiacek, B.A. Korgel. Supercritical fluid–liquid–solid synthesis of gallium arsenide nanowires seeded by alkanethiol-stabilized gold nanocrystals. *Adv. Mater.*, **16**, 646 (2004).
[10] P.S. Shah, T. Hanrath, K.P. Johnston, B.A. Korgel. Nanocrystal and nanowire synthesis and dispersibility in supercritical fluids. *J. Phys. Chem. B*, **108**, 9574 (2004).
[11] D.C. Lee, F.V. Mikulec, B.A. Korgel. Carbon nanotube synthesis in supercritical toluene. *J. Am. Chem. Soc.*, **126**, 4951 (2004).
[12] C.L. Yaws. *Handbook of Thermodynamic Diagrams*, p. 294, Gulf Publishing Company, Houston, TX (1996).
[13] A. Burian, J.C. Dore, H.E. Fischer, J. Sloan. Structural studies of mutliwall carbon nanotubes by neutron diffraction. *Phys. Rev. B*, **59**, 1665 (1999).
[14] M. Kociak, L. Henrard, O. Stephan, K. Suenaga, C. Colliex. Plasmons in layered nanospheres and nanotubes investigated by spatially resolved electron energy-loss spectroscopy. *Phys. Rev. B*, **61**, 13936 (2000).
[15] K. Zeppenfeld. Anisotropic plasmon behavior in graphite. *Phys. Lett.*, **25A**, 335 (1971).
[16] L.J.E. Hofer, E. Sterling, J.T. McCarthy. Structure of the carbon deposited from carbon monoxide on iron, cobalt and nickel. *J. Phys. Chem.*, **59**, 1153 (1955).
[17] J.R. Bradley, Y.L. Chen, H.W. Sturner. The structure of carbon filaments and associated catalytic particles formed during pyrolysis of natural-gas in steel tubes. *Carbon*, **23**, 715 (1985).
[18] Z.F. Ren, Z.P. Huang, J.W. Xu, J.H. Wang, P. Bush, M.P. Siegal, P.N. Provencio. Synthesis of large arrays of well-aligned carbon nanotubes on glass. *Science*, **282**, 1105 (1998).
[19] L. Delzeit, C.V. Nguyen, B. Chen, R. Stevens, A. Cassell, J. Han, M. Meyyappan. Multiwalled carbon nanotubes by chemical vapor deposition using multilayered metal catalysts. *J. Phys. Chem. B*, **106**, 5629 (2002).
[20] D.S. Bethune, C.H. Kiang, M.S. Devries, G. Gorman, R. Savoy, J. Vazquez, R. Beyers. Cobalt-catalyzed growth of carbon nanotubes with single-atomic-layerwalls. *Nature*, **363**, 605 (1993).
[21] M. Yudasaka, R. Kikuchi, T. Matsui, Y. Ohki, S. Yoshimura, E. Ota. Specific conditions for Ni catalyzed carbon nanotube growth by chemical-vapor-deposition. *Appl. Phys. Lett.*, **67**, 2477 (1995).
[22] X. Wang, W.B. Yue, M.S. He, M.H. Liu, J. Zhang, Z.F. Liu. Bimetallic catalysts for the efficient growth of SWNTs on surfaces. *Chem. Mater.*, **16**, 799 (2004).
[23] H.W. Pollack. *Materials Science and Metallurgy*, Englewood Cliffs, New York (1988).
[24] R.T.K. Baker. Catalytic growth of carbon filaments. *Carbon*, **27**, 315 (1989).
[25] G.G. Tibbetts, M.G. Devour, E.J. Rodda. An adsorption-diffusion isotherm and its application to the growth of carbon filaments on iron catalyst particles. *Carbon*, **25**, 367 (1987).
[26] C.L. Cheung, A. Kurtz, H. Park, C.M. Lieber. Diameter-controlled synthesis of carbon nanotubes. *J. Phys. Chem. B*, **106**, 2429 (2002).
[27] K.J. Ziegler, R.C. Doty, K.P. Johnston, B.A. Korgel. Synthesis of organic monolayer-stabilized copper nanocrystals in supercritical water. *J. Am. Chem. Soc.*, **123**, 7797 (2001).